Ceramics-Silikáty 66 (3), 384-395 (2022)
www.ceramics-silikaty.cz doi: 10.13168/cs.2022.0034

EXPERIMENTAL VERIFICATION OF THE NEW MODELS APPLIED TO GLASS FIBRE REINFORCED CONCRETE (GFRC) CONFINED WITH GLASS FIBRE REINFORCED POLYMER (GFRP) COMPOSITES

#DJARIR YAHIAOUI*, BELGACEM MAMEN**, MOHAMED SAADI*, TAYEB BOUZID*

*LGC-ROI, Civil Engineering Laboratory-Risks and Structures in Interactions, Department of Civil Engineering, Faculty of Technology, University of Batna 2, Batna 05001, Algeria
**Department of Civil Engineering, Faculty of Science and Technology, Abbès Laghrour University, Khenchela 40000, Algeria

#E-mail: d.yahiaoui@univ-batna2.dz

Submitted May 14, 2022; accepted July 21, 2022

Keywords: Axial compression, Circular columns, GFRP, Confinement model, Crack propagation

External confinement by the GFRP composites offers an actual process for retrofitting glass fibre reinforced concrete columns (GFRC) subject to static or seismic loads. This paper presents an experimental investigation and analytical modelling of the axial compression of confined circular concrete columns of different strengths (8.5, 16, and 25 MPa). Furthermore, the columns contain different percentages of glass fibres (0.3 to 1.2 %), and their confinement is given by GFRP composites of various thicknesses (0.8 to 2.4 mm). The uniaxial compression test on these specimens reveals that the glass fibre percentage and the thickness of the GFRP play a vital role in improving the load-deformation behaviour and crack propagation. Whatever the concrete strength, the ultimate axial strain and stress predicted using the suggested confinement model almost agrees with the available experimental results.

INTRODUCTION

Nowadays, concrete is the main building material in the world. There is a slight concern that concrete will remain a construction material due to its benefits, such as its high strength, sturdy deformation resistance, and low cost. However, concrete has a particular fragility, poor performance in terms of ductility, and reduced crack resistance. More importantly, it easily cracks due to its low tensile strength, which causes a faster failure after the first indications of fracture [1–3]. Hence, the need to develop new processes offers the opportunity to overcome these limitations.

Researchers have reported that randomly distributed concrete fibres mainly reduce the crack propagation and improve the aforementioned imperfections [4-6]. The traction forces acting on the cracks are carried by the fibres, strengthening the concrete matrices and supporting the traction load, preventing further crack development. As a result, when compared to conventional concrete, fibre-reinforced concrete has improved properties, bending resistance, shock strength, elongation, and ductility. It also has properties that prevent shrinkage, breaking, freezing, and corrosion. Steel fibres [7-9], carbon fibres [10-11], polypropylene fibres [12-13], basalt fibres [14-15], glass fibres, [16-17] and vegetal fibres [18-19] are just some examples of the fibres that can be utilised. According to these research studies, the fibre type should be carefully chosen depending on the job's specifications.

As the fibre volume increases, the tensile and compressive strengths firstly increase, then decrease. Furthermore, shorter fibres have proven to be more beneficial to longer fibres. As a result, different fibres have various impacts on the mechanical and physical properties. For example, tiny flexible fibres have also proven to be more effective at limiting the initiation of microcracks. On the other hand, large, stiff fibres are better at controlling the growth of cracks [20]. Though, the mechanical resistance does not always increase with the percentage and mechanical properties of the incorporated fibre, implying that there are ideal fibre parameters to achieve maximum the mechanical strength [21]. The type of fibre determines the optimum glass fibre percentage. In general, shorter fibres with higher length diameter metrics are more effective at regulating the formation of small cracks. Despite this, longer fibres with a reduced length diameter percentage are more efficient at monitoring the evolution of microcracks. As a result, incorporating multiple fibres could create a notable impact. For illustration, the mixture of polyvinyl alcohol (PVA) and steel fibres aids in achieving the optimal tensile behaviour. Also, it was demonstrated that incorporating adequate quantities of basalt fibres limited the porous structure of the concrete and, thus, enhanced its longevity [22-23].

Nevertheless, combining different types of fibres does not significantly improve the tensile strength of reinforced concrete. Therefore, the glass fibre reinforced

concrete (GFRP) composites' external confinement has been proposed as a creative solution to overcome this barrier. Due to the external confinement of Fibre Reinforced Polymers (FRPs), when concrete dilates non-linearly due to the formation of internal cracks, the dilation speed rapidly increases to a peak value before stabilising at a lower value. Previous research showed that severely confined concrete has almost no volumetric expansion [24-27]. The concrete dilation, which engages the FRP confining pressure, greatly depends on the stiffness of the confining material. Furthermore, stiff FRP confined concrete will certainly show lower dilation than flexible FRP confined concrete. For repair and strengthening, where ductility enhancement is a central objective, a flexible FRP is generally more beneficial as it makes the material more ductile [28]. These studies did not investigate the behaviour of glass fibre-containing concrete (GFCC) specimens in which the lateral expansion is uneven around the border.

With this background, available studies concerning the behaviour of confined concrete are mostly limited to unreinforced concrete; information on glass fibre-containing concrete wrapped with an FRP jacket is very scarce and unclear. Moreover, models for predicting the ultimate axial strain and the compressive strength of glass fibre-containing concrete wrapped with an FRP jacket are vague because there is no relevant published study, to the best of the authors' knowledge, at the time of writing this paper. From this perspective, the present study evaluates the effect of the concrete strength, glass fibre percentage, and the GFRP layer thickness on the strength properties, failure mechanism, and the axial strength-strain behaviour of GFCC cylinder specimens externally confined with GFRPs. The performance of the proposed confinement model and those existing in the literature has been assessed using the database collected in this study, which aimed to provide a reference for predicting the ultimate axial strain and the compressive strength of glass fibre-containing concrete wrapped with an FRP jacket.

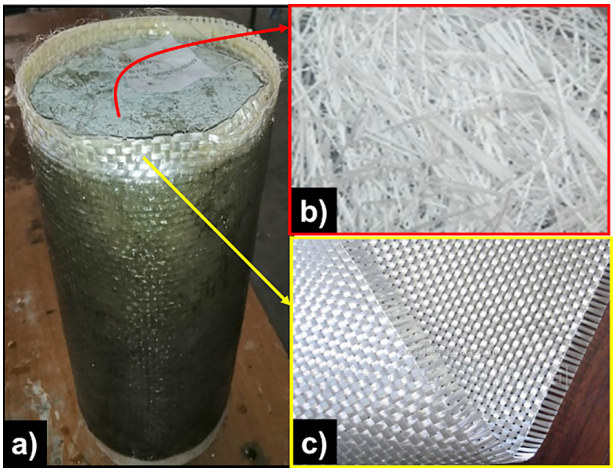

Figure 1. GFRP strengthened specimens (a); glass fibre (b); GFRP composites (c).

EXPERIMENTAL

Materials and sample preparation

Three commercial materials were considered to elaborate the confined circular concrete columns, see Figure 1a. The first material is Portland cement, used as a binder to obtain three different strengths. Its physical properties are summarised in Table 1. For crack control in *in situ* concrete and to improve the toughness of the concrete, alkali-resistant glass fibres have been used with different percentages (0, 0.3, 0.6, 0.9, and 1.2 wt. %) for the preparation of the glass fibre reinforced concrete, see Figure 1b and Table 2. For the retrofit of glass fibre reinforced concrete columns subjected to either static or seismic loads, external confinement by the GFRP composites can be considered an actual process. For this purpose, local polyester resin and bidirectional fibre-glass were used to develop a low-cost glass fibre reinforced polymer composite (see Figure 1c). In the boating industry, this category of bi-directional fibre-glass is commonly used. For the confinement of GFRC columns, glass FRP composites of various thicknesses (0.8 to 2.4 mm) were prepared and tested using the UTS-SHIMADZU universal machine according to the standard guidelines of ASTM D638 (2010) [29]. For each thickness, three tensile samples were tested to obtain accurate results.

Primarily, the cement, sand, gravel, and fibre were added to a suitable amount of water and mixed until the fibres were sufficiently dispersed. The mixture was then cast into 150 mm diameter cylindrical moulds having 300 mm in height. First, the polyester resin was applied to the sample's external surface with a brush, and then a resin-soaked fibre-glass board was covered around the circular concrete cylinder. The concrete surface was

Table 1. Raw materials in (wt. %) for the used concretes.

Concrete	CS-8.5	CS-16	CS-25
Cement (kg·m^{-3})	200	300-3	400
Sand (kg·m^{-3})	853	810	773
Coarse aggregate (kg·m^{-3})	853	520	496
Fine aggregate (kg·m^{-3})	481	520	496
Water (kg·m^{-3})	100	132	163
Superplasticiser		as required	
Compressive strength (MPa)	8.5	16	25

Table 2. Characteristics of the glass fibre and GFRP composites.

Material and characteristics	Glass fibre (alkali-resistant)	GFRP composites	
		Epoxy resin	GFRP
Length (mm)	3–4.5	–	–
Filament diameter (mm)	0.015	–	–
Tensile strength (MPa)	1500–1700	17.20	377.64
Elastic modulus (MPa)	72	2.72	18.70
Density (kg·m^{-3})	2600	–	–
Ultimate strain (%)	–	0.6322	0.00204
Standard deviation	1.08	–	1.91

adequately cleaned to remove dust before applying the GFRP compound. Second, the GFRP composites were applied after 28 days. The final strengthened specimen is shown in Figure 1a.

Test procedure

The behaviour of glass fibre-containing concrete confined by GFRP composites under compression load were examined to assess the suitability of this innovative composite material. For this research plan, 96 circular concrete columns were constructed and analysed (Figure 1). To record the axial deformation, three linear variable differential transducers (LVDTs) were vertically mounted on a specially designed steel frame, as shown in Figure 1. Threaded bolts connect the steel frame to the concrete cylinders. Also, as shown in Figure 1, two strain gauges are horizontally placed at the mid-height of the concrete cylinders to report the lateral dilation of the confined sample. A pre-calibrated hydraulic jack with a capacity of 2000 kN was used to apply the monotonic axial load at a constant stroke rate of 0.1 KN·s^{-1}. Before applying the load, the top and bottom surfaces of the concrete cylinders were cleaned, ground, and covered with high-strength gypsum to ensure the uniform application of the load over the entire area. The gypsum cap was also cut off over the GFRP jackets to prevent the axial load transmission to the GFRP jackets. The investigation is mainly based on analysing the effect of the type of concrete, the layer thickness of the GFRP composite, and the proportion of the fibre reinforcement in the concrete.

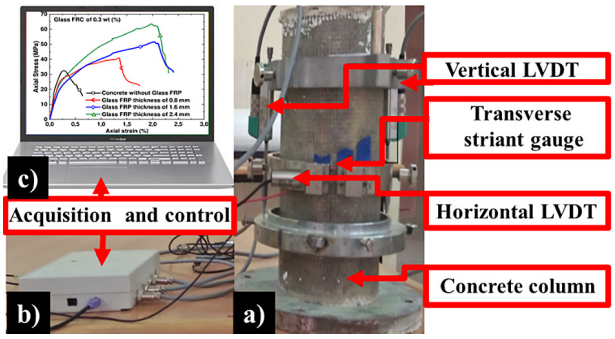

Figure 2. Experimental set-up for the uniaxial compression testing of the GFRP strengthened concrete columns.

RESULTS AND DISCUSSION

Effect of reinforcement on the uniaxial compression behaviour

Different uniaxial compression tests were carried out to analyse the influence of the glass fibre percentage and FRP composite thickness on the mechanical behaviour of the reinforced concrete. The associated stress-strain curves obtained are shown in Figures 3 and 4. For the specimens without the glass FRP, the strength of the material increases with the increasing glass fibre percentage up to 0.9 wt. %. Beyond this percentage, the material strength decreases to a minimum value. Also, for the percentage of 1.2 wt. %, the specimens with the glass FRP exhibit minimal strength. Therefore, the progress of the curves, see Figure 3a-d, demonstrates two behavioural trends. First, the glass fibre-containing concrete (GFCC) displays a quasi-brittle behaviour where the curves are almost linear up to the maximum stress. The stress-strain curves suddenly decrease after reaching the maximum value, generally due to a brittle fracture, Figure 3a.

Second, for specimens with the glass FRP composites, the stress-strain curves are open bell-shaped, and the material's ductility increases, see Figure 3b-d. Also, the axial strains developed by the reinforced concrete at the peak stress are increased. Notably, the stress level remains relatively constant over an extensive strain range and decreases slowly toward a significant deformation confirming the strain hardening behaviour, see Figure 3b-d. This behaviour is evident, as shown in Figure 4a-d.

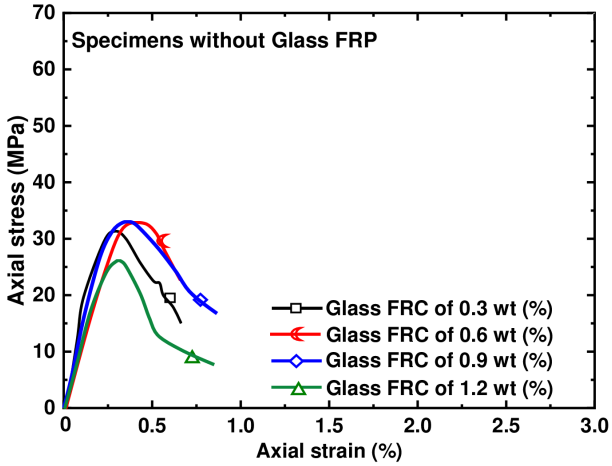

a) 0 mm

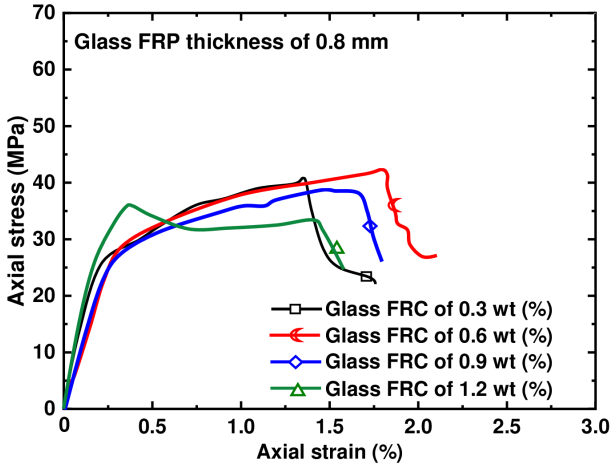

b) 0.8 mm

Figure 3. Typical stress-strain curves of the strengthened and confined strengthened samples with different GFRP thicknesses: a) 0 mm, b) 0.8 mm. *(Continue on next page)*

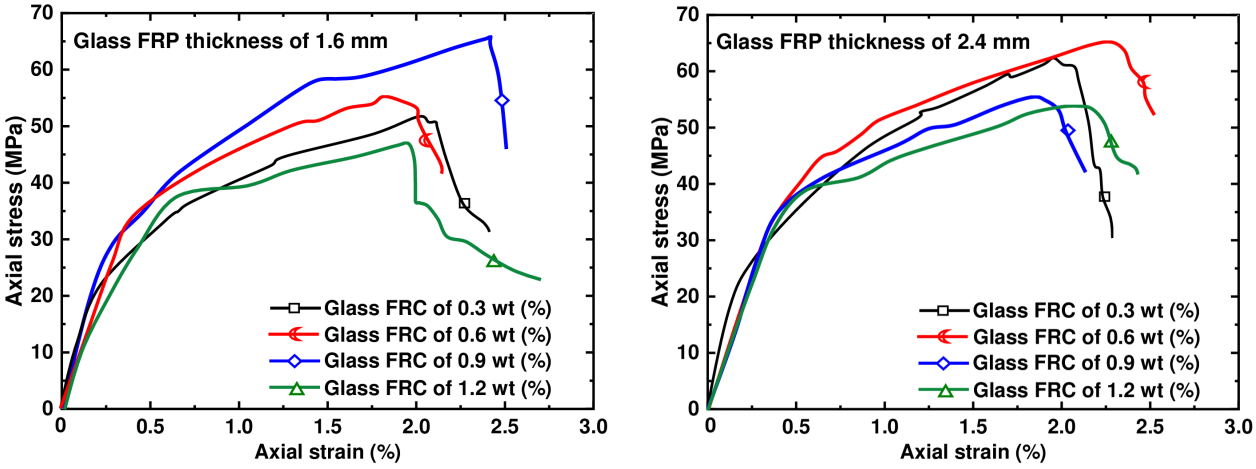

c) 1.6 mm d) 2.4 mm

Figure 3. Typical stress-strain curves of the strengthened and confined strengthened samples with different GFRP thicknesses: c) 1.6 mm and d) 2.4 mm.

The increase in the strength is linearly related to the increase in the glass FRP thickness. Significantly, the concrete dilation is enough to engage the required FRP confining pressure. Therefore, this dilation generates an increase in the strength. This ductility enhancement is a required parameter for repairing and strengthening

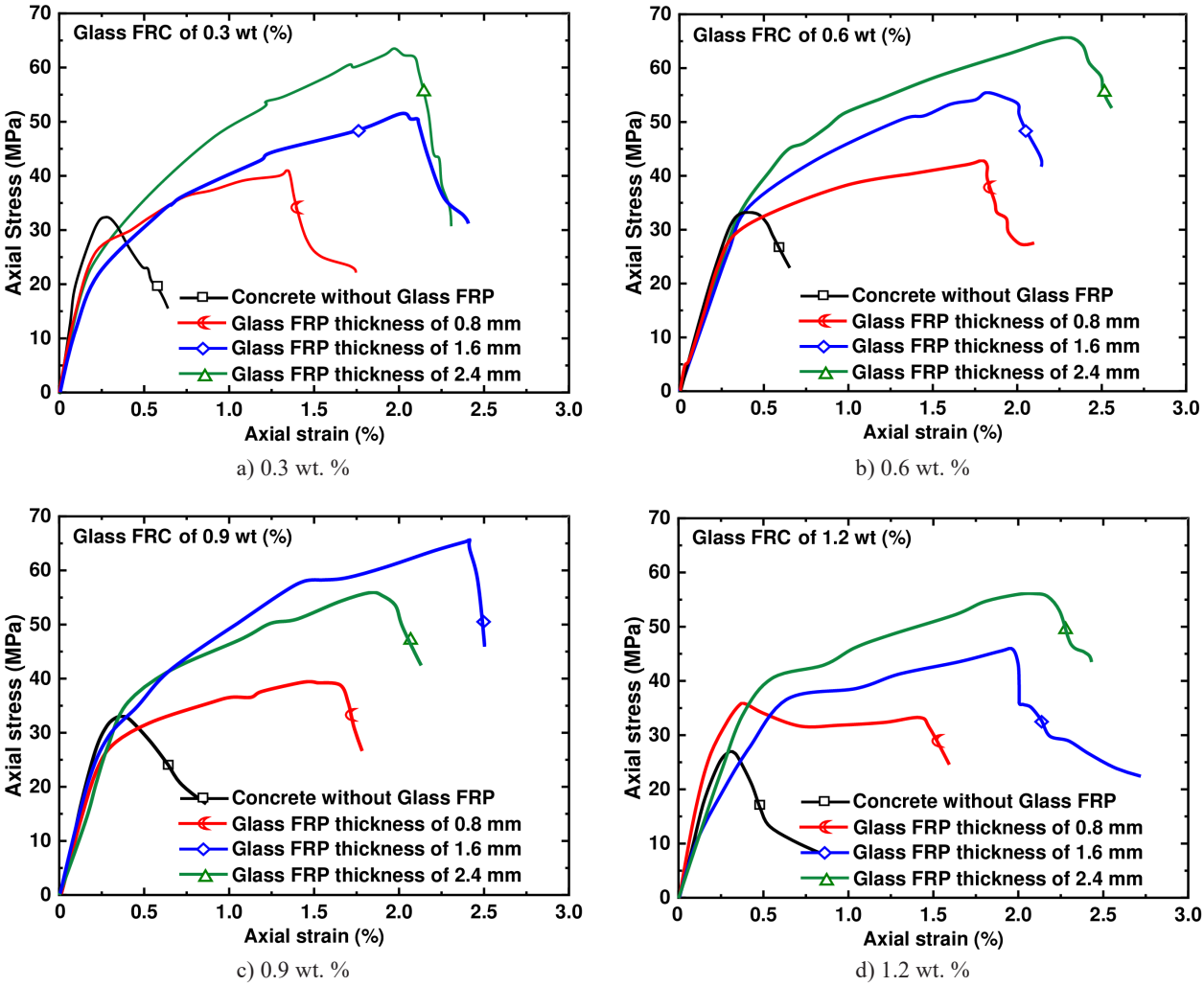

a) 0.3 wt. % b) 0.6 wt. %

c) 0.9 wt. % d) 1.2 wt. %

Figure 4. Typical stress-strain curves of the unconfined and confined strengthened samples with different percentages of GFRC: a) 0.3 wt. %, b) 0.6 wt. %, c) 0.9 wt. % and d) 1.2 wt. %.

structures. One can conclude that the percentage of glass fibre does not determine the optimal thickness of the glass FRP.

Effect of the reinforcement on the mechanical features

Figures 5a-d display the influence of the glass fibre percentage on the increasing reinforcement factor (IRF) determined analytically based on the uniaxial compression strengths. The increasing reinforcement factor represents the fibre-reinforced concrete strength ratio to the unreinforced value. The recorded data were the average values of three tests at each temperature. Whatever the concrete strength, the general trend of the curves is almost similar. The increasing reinforcement factor values increase when the glass fibre ranges between 0 and 0.6 wt. %. Beyond 0.6 wt. %, a sharp decrease in the IRF is observed. These observations show that the GFCC samples containing 0.6 wt. % of FRP give generally higher values of stress and strain than all the other samples.

The increasing confinement factor (ICF) evolution is illustrated in Figure 6a-d for the glass FRP thickness using different strength values. The calculated data are the average values of three tests. The increasing confinement is more significant for the GFRC samples confined with a thick (2.4 mm) GFRP. High values of ICF are due to the fact that the unreinforced concrete, as a brittle material, generally has a lower compression strength than the reinforced concrete confined with the GFRP composites.

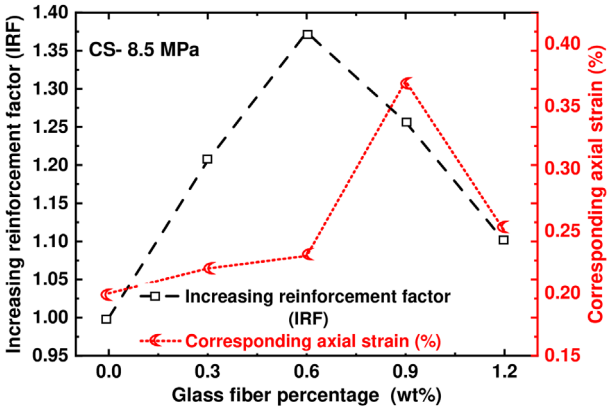

a) 8.5 MPa

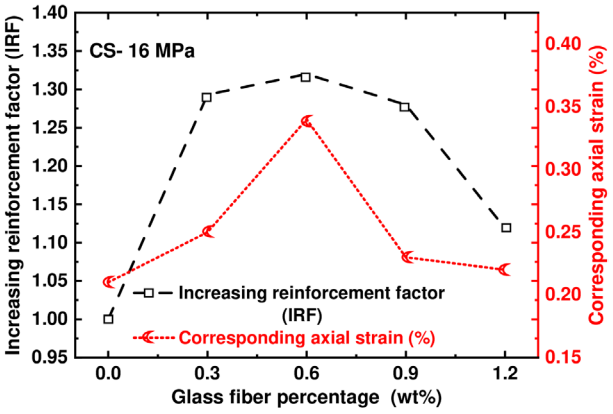

b) 16 MPa

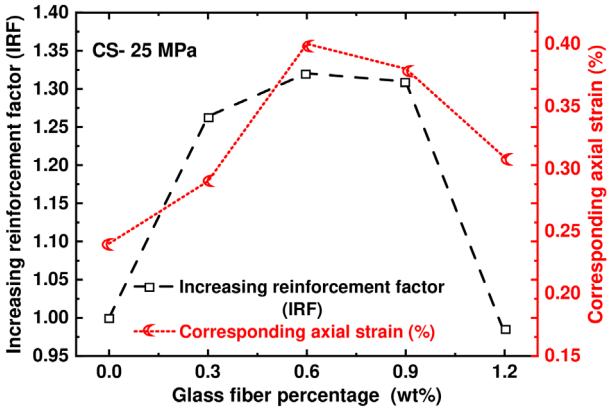

c) 25 MPa

Figure 5. Increasing reinforcement factor vs. glass fibre percentage for the different GFRC percentages and concrete strengths: a) 8.5 MPa, b) 16 MPa and c) 25 MPa.

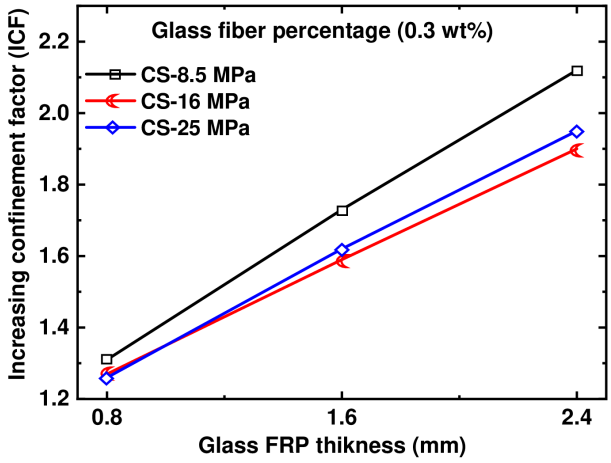

a) 0.3 wt. %

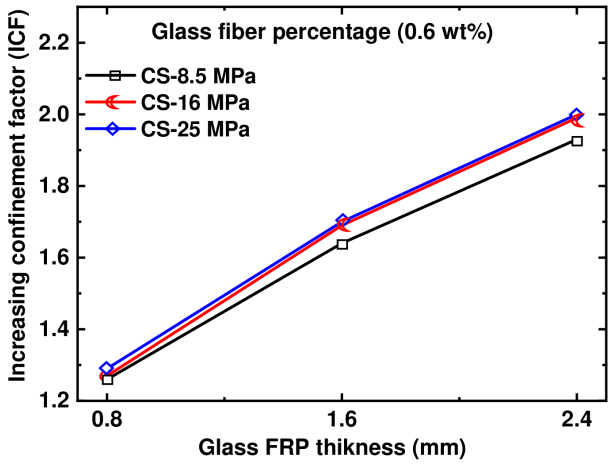

b) 0.6 wt. %

Figure 6. Increasing confinement factor vs. glass FRP thickness for the different concrete strengths: a) 0.3 wt. %, b) 0.6 wt. %.
(Continue on next page)

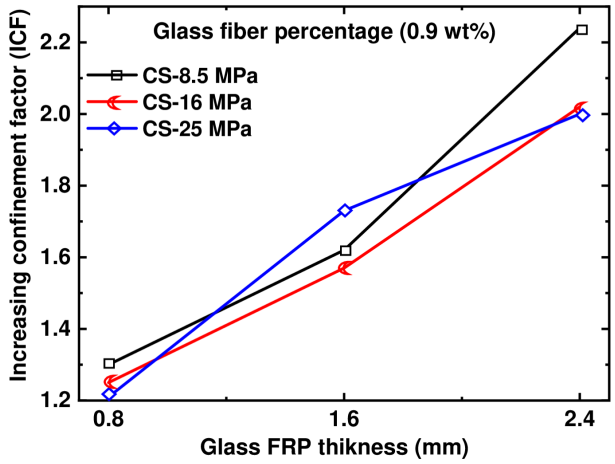

c) 0.9 wt. %

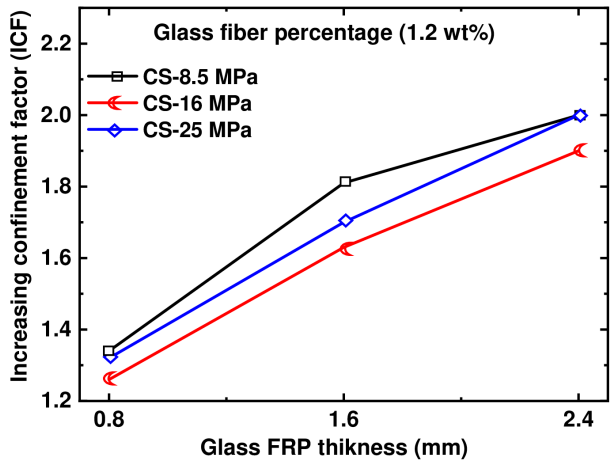

d) 1.2 wt. %

Figure 6. Increasing confinement factor vs. glass FRP thickness for the different concrete strengths: c) 0.9 wt. %, d) 1.2 wt. %.

However, the influence of GFRP is independent of both the glass fibre percentage and the material strength. It is concluded that: the GFRP confinement on the low-strength concrete specimens (8.5 MPa) produces higher results in terms of the increasing con-finement than for the high-strength concrete similar specimens (8.5 MPa).

Failure compression behaviour

Many researchers have confirmed that the failure modes of ordinary concrete are the sudden collapse after an extreme load. They are highly destructive due to the material cracking at the central location [30]. Figure 7a-c shows an illustration of the crack propagation pattern and failure mode of GFCC with 0.9 wt. % fibre for three strengths (25 MPa, 16 MPa, 8.5 MPa). The presence of the glass fibres prevents the complete crushing of the specimens. The percentage of glass fibres lead to an increase in the stability of the concrete at failure (Figure 7a-c). Longitudinal and transverse failure patterns were observed for all the specimens, and they did not show diagonal cone-type failures. Even with a high strength (Figure 7a), the interfacial bonds between the glass fibre and the cement paste could fail, due to the poor interfacial transition, causing void generation and, consequently, ease of failure.

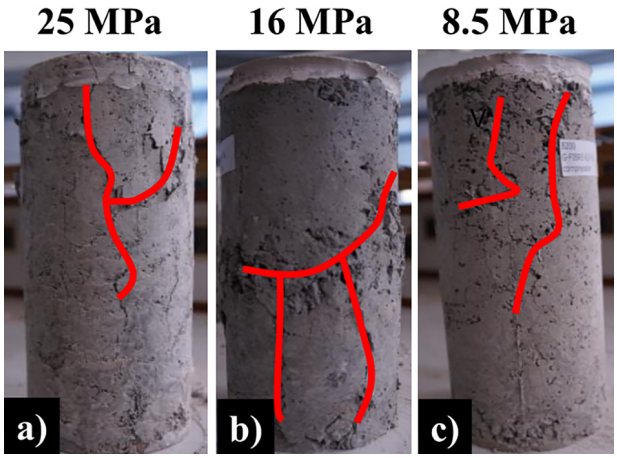

Figure 7. Failure modes of the glass fibre reinforced concrete (GFRC).

Figure 8a-i shows the ultimate failure modes of the glass fibre reinforced concrete with different strengths (8.5, 16, and 25 MPa) and confined with the glass FRP composite of different thicknesses (0.8, 1.6, and 2.4 mm). In the first and intermediate loading stages, the experimental phenomena of all the test specimens are similar under axial load. The difference is only in the last stage of loading. In Figure 8a-c, it is noted for the GFRC-GFRP confined specimens that the ultimate failure modes are mainly observed at the mid-height of all the concrete cylinders as large and long longitudinal failure patterns. Such a propagation pattern is mainly due to the tensile rupture of the GFRP jackets.

The transversal crack is large, but no longer like the previous one shown in Figure 8a-c. More importantly, thin transversal failure patterns appear on the side of all the GFRC-GFRP samples, and they do not go all the way around. Such thin horizontal cracks are due to the relatively low pressure applied by the GFRP jackets with a 0.8 mm thickness. As the thickness of the GFRP jackets increases (0.8 mm, see Figure 8d-f), the failure mechanism can also be identified at the mid-height with longitudinal and transversal failure patterns.

These cracks opened up due to the high pressure activated by the thick glass FRP composite. Also, they confirm the strain hardening behaviour shown in Figure 3. However, for glass fibre reinforced concrete confined with the thick glass FRP composite, the failure mechanism is identified at the mid-height no longer with longitudinal failure and thick transversal failure patterns, see Figure 8g-i.

In the end, the ultimate failure mode is greatly affected by the confinement thickness. Thus, the GFRC specimens with lower GFRP thickness have a concealed

strain hardening behaviour. In contrast, the GFRC specimens confined under higher GFRP thickness tend to exhibit an evident strain hardening behaviour.

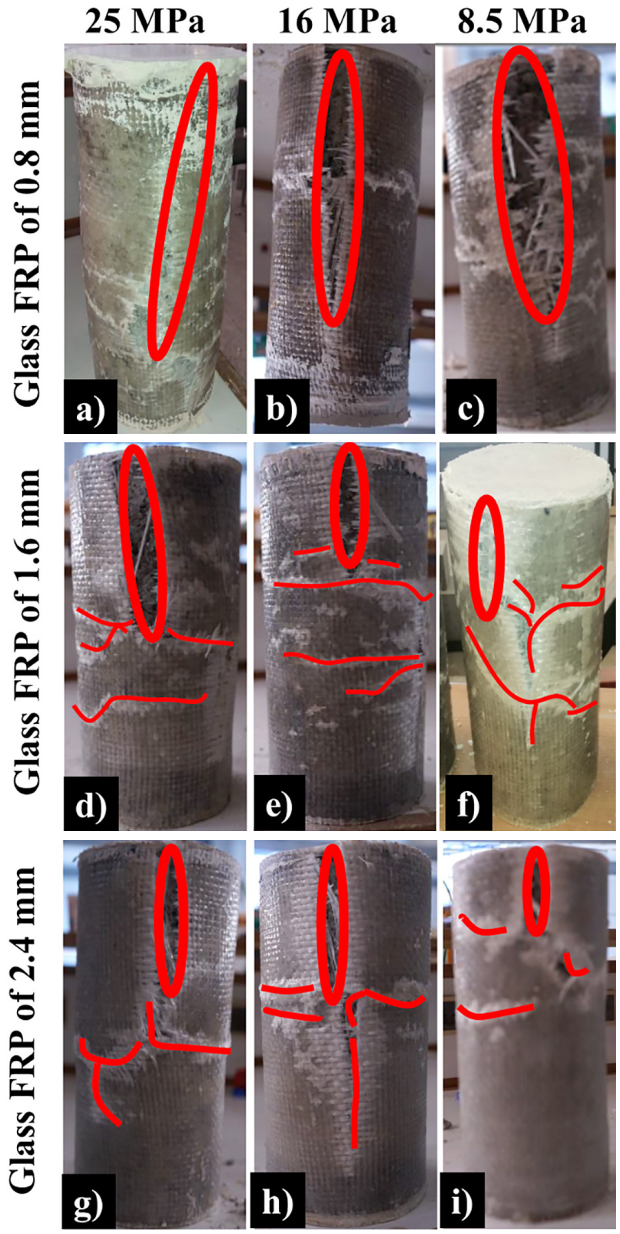

Figure 8. Failure modes of the glass fibre reinforced concrete (GFRC) confined with glass FRP composites.

Confinement modeling and results

Assessment of the existing models

Generally, the axial stress versus axial strain behaviour of FRP confined circular concrete specimens is an ascending one. The first part is usually linear and identical to the unconfined concrete's axial stress-strain response. The second part of stress versus axial strain is mainly considered a transition zone. The third part is once again linear, similar to the first part; however, the stiffness of the third part is usually much lower than the first part.

Figure 9 presents the reliability of the strength models of the unconfined and FRP confined specimens through the axial stress versus strain. The terms f_{cu} and ε_{cu} are the ultimate axial stress and the axial strain of the unconfined concrete, respectively. In contrast, the terms f_{cc} and ε_{cc} are the ultimate axial stress and the axial strain of the FRP confined concrete, respectively.

For the design of the FRP confined concrete models, f_{cc} and ε_{cc} are used in the theoretical and finite element analysis. In the existing literature [31], the terms f_{cc} and ε_{cc} are related to f_{cu} and ε_{cu}, respectively, in the following equations:

$$f_{cc} = \left[1 + C_e\left(\frac{F_l}{f_{cu}}\right)\right] f_{cu} \quad (1)$$

$$\varepsilon_{cc} = \left[1 + S_e\left(\frac{F_l}{f_{cu}}\right)\right] \varepsilon_{cu} \quad (2)$$

where C_e and S_e are the confinement effectiveness and strain enhancement coefficients, respectively. In this study, the experimental results are used to evaluate the performance of the current ultimate stress and strain models of the GFCC confined GFRP state. The selected existing ultimate stress and strain confinement models are specified in Table 3. They have been developed mainly for various FRP composites, such as carbon FRP (CFRP) and glass FRP (GFRP) for low or high-strength concrete.

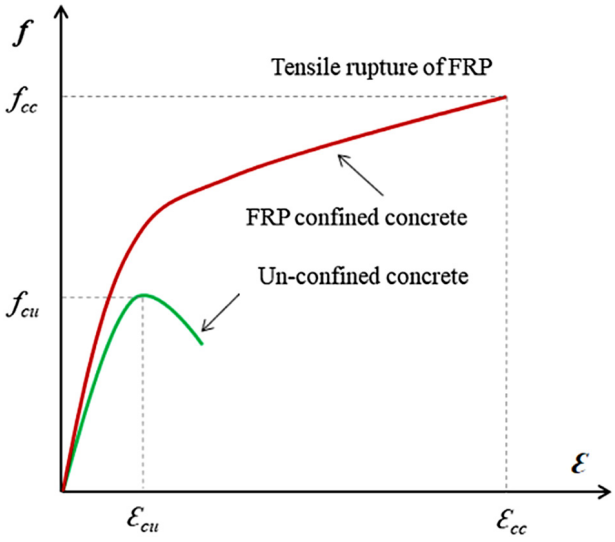

Figure 9. Performance of the strength models.

Proposed strength model for the GFRP confined GFCC cylinder concrete columns

The ultimate axial stress f'_{cc} and strain ε'_{cc} are of particular importance to the stress-strain model; a strong (linear) correlation was found between the ratio of f'_{cc}/f_{co} to the ratio of f_l/f_{co} primarily based on testing the GFRP confined GFCC cylinders.

Table 3. Selected models for the ultimate strength and strain.

Model	Ultimate stress	Ultimate strain
Ghernouti et al. [32]	$f_{cc}=\left[1+2.023\left(\frac{F_l}{f_{co}}\right)\right]f_{co}$	$\varepsilon_{cc}=\left[1+10.63\left(\frac{F_l}{f_{co}}\right)\right]\varepsilon_{co}$
Benzaid et al. [33]	$f_{cc}=\left[1+2.20\left(\frac{F_l}{f_{co}}\right)\right]f_{co}$	$\varepsilon_{cc}=\left[1+7.60\left(\frac{F_l}{f_{co}}\right)\right]\varepsilon_{co}$
Teng et al. [34]	$f_{cc}=\left[1+3.5\left(\frac{F_l}{f_{co}}\right)\right]f_{co}$	$\varepsilon_{cc}=\left[1+17.50\left(\frac{F_l}{f_{co}}\right)\right]\varepsilon_{co}$
Liao et al. Liao [35]	$\frac{f_{cf}^{'}}{f_{co}}=1.0+0.606\left(\frac{f_{l,a}}{f_{co}}\right)^{0.6}\left(\frac{\varepsilon_{h,rup}}{\varepsilon_{co}}\right)^{0.6}$	$\frac{\varepsilon_{cc}}{\varepsilon_{co}}=1.0+0.595\left(\frac{f_{l,a}}{f_{co}}\right)^{0.1}\left(\frac{\varepsilon_{h,rup}}{\varepsilon_{co}}\right)^{1.45}$

Rather than observing a linear relationship, it was found that the rate of increase of f'_{cc}/f_{co} decreases as f_l/f_{co} increases. Consequently, the ultimate stress and ultimate strain was firstly determined by the effective lateral confinement offered by the GFRP wrap and hoop reinforcement. Based on a multi-parameter regression analysis of the 96 results contained in the test database, the following equation for the ultimate stress is proposed and for which the correlation coefficient (R^2) is 0.9993.

$$f_{cc}=0.847f_{cu}-0.14f_l+0.1f_l\times f_{cu} \quad (3)$$

where the confining pressure f_l is estimated as follows:

$$f_l=\frac{2f_f t}{d}$$

where f_f is the tensile strength of the FRP determined from the flat coupon tests, t is the thickness of the FRP, and d is the section diameter.

Verification of the strength model

In order to verify the validity of the proposed model, the prediction results of f'_{cc}/f_{co} were compared with four existing theoretical models [32-35]. Figure 10 shows the comparisons of the test results and predictions of f'_{cc}/f_{co} for the GFRP confined GFCC.

The average prediction of the test results for the strength of 25 MPa are –2 %, –5 %, –8 % and –13 % for the Teng et al. [34], Benzaid et al. [33], Ghernouti, and Rabeh [32], and Liao et al. [35] models, respectively. For the strength of 16 MPa, the test results are estimated to be around 13 % to 23 % on average for the Teng et al. [34], Benzaid et al. [33], Ghernouti, and Rabeh [32] models and 52 % for the Liao et al. [35] model. At the lower strength case of 8.5 MPa, the models overestimate the test results in most cases, estimating 54 % to 70 %. The prediction effect of the four existing theoretical models for the specimens is satisfied for a strength of 25 MPa, but it significantly increases the strength enhancement of the specimens with a strength of 16 and 8.5 MPa. The present study offers reasonable predictability as most data points are close to the diagonal. Therefore, a maximum error of –1 % is noted for the prediction of f'_{cc}/f_{co}. The proposed model appears to be more accurate in predicting f'_{cc}/f_{co}.

Figure 11 summarises the data graphically. It can be seen that the prediction of f'_{cc} by the proposed model has the best AAE, MSE, and SD for all data sets.

Proposed strain model for GFRP confined GFCC cylinders concrete columns

On the basis of a multi parameter regression analysis of the 96 results contained in the test database, Equation 4 takes the effect of the confinement stiffness and glass fibre percentage on the ultimate axial strain into account as follows:

$$\frac{\varepsilon_{cc}^{'}}{\varepsilon_c}=-6.5\left(\frac{f_c^{'}}{\varepsilon_c}\right)^{0.1}+1.37\left(\frac{f_l}{\varepsilon_c}\right)^{0.3}+5.07\left(\frac{\varepsilon_{cch}^{'}}{\varepsilon_c}\right)^{0.3}-1.17 \quad (4)$$

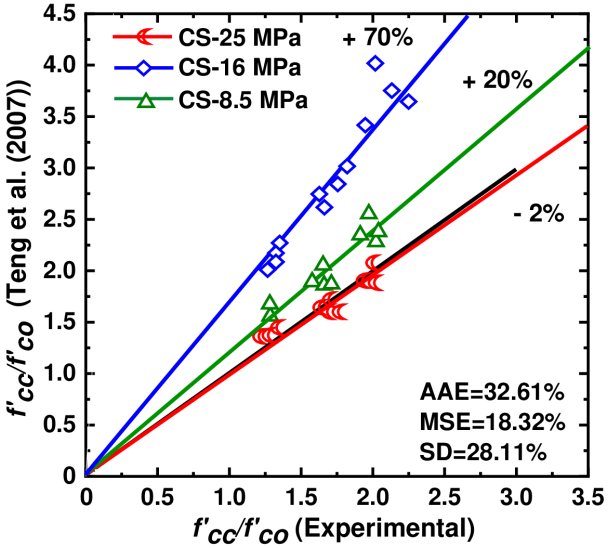

a) Teng et al (2007)

Figure 10. Comparison of the selected strength models with the experimental results. *(Continue on next page)*

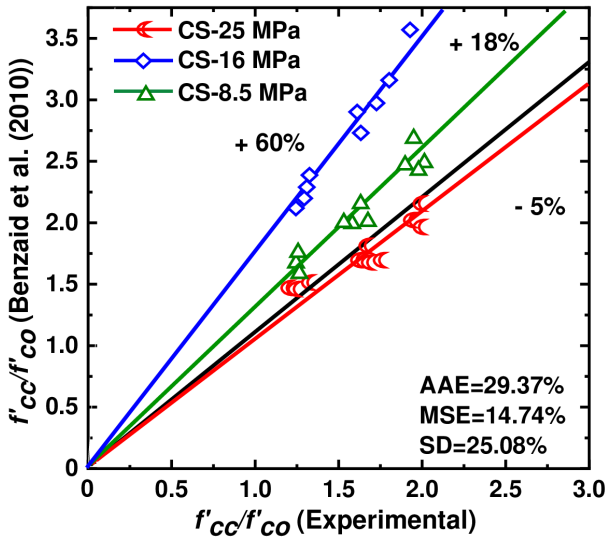

b) Benzaid et al (2010)

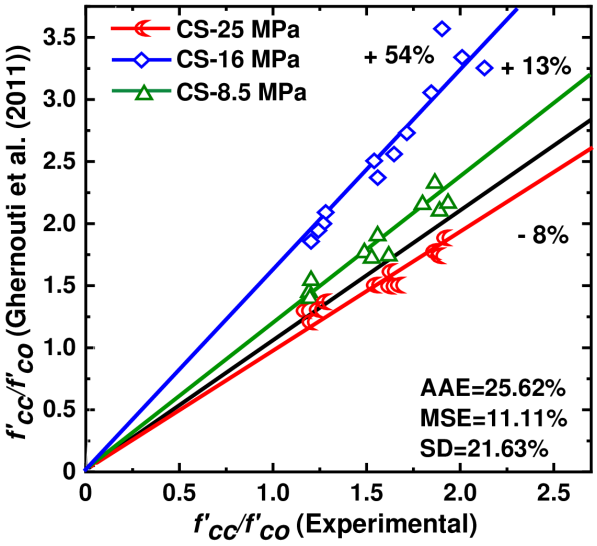

c) Ghernouti et al (2011)

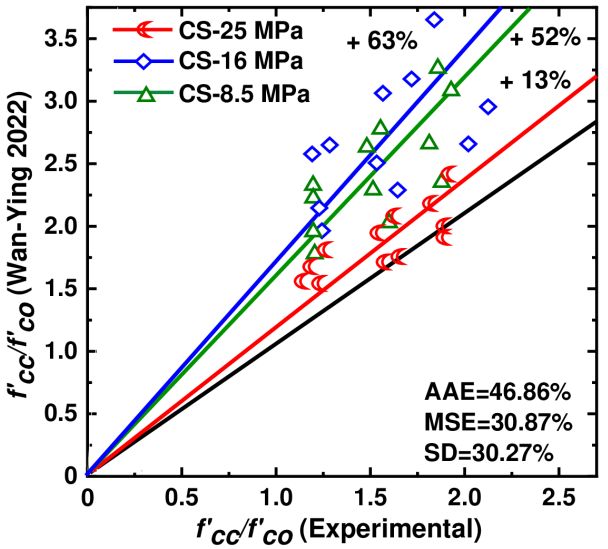

d) Wan-Ying 2022

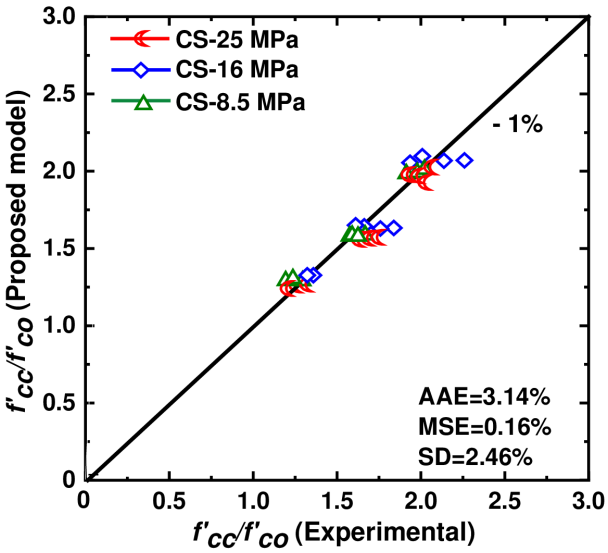

e) proposed model

Figure 10. Comparison of the selected strength models with the experimental results.

The ultimate strain ε'_{cc} is of particular importance to the stress-strain model, where a strong (linear) correlation between the ratio of $\varepsilon_{cc}/\varepsilon_{co}$ to the ratio of f_l/ε_c, f'_c/ε_c and $\varepsilon'_{cch}/\varepsilon_c$ was found primarily on the basis of testing the GFRP confined GFCC cylinders.

Verification of the strain model

Figure 12 shows the theoretical model's strain versus experimental strain of the GFRP confined GFCC cylinders, and the three statistical indictors (AAE, MSE, and SD) are also labelled in each comparison. As seen in the models of Teng et al. (2007) [34], Benzaid et al. [33], Ghernouti and Rabehi [32], and Liao et al. [35], it give a maximum error between –28 % to +280 %, ± 56.2 %, 54 % to +82 % and –64 % to +56 %, respectively. After

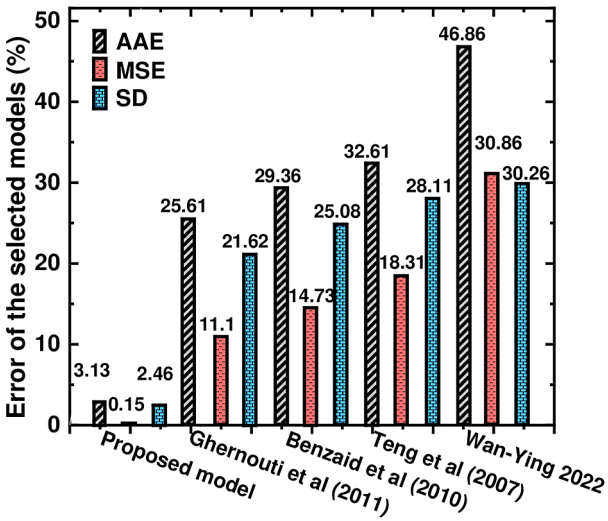

Figure 11. Evaluation parameters in predicting the normalised ultimate strength.

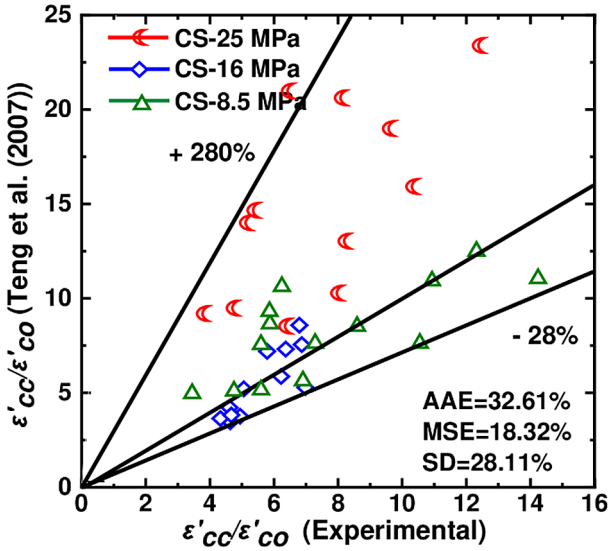

a) Teng et al (2007)

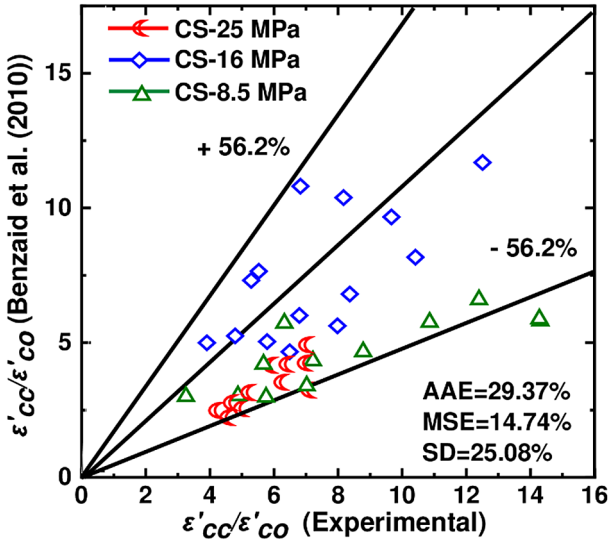

b) Benzaid et al (2010)

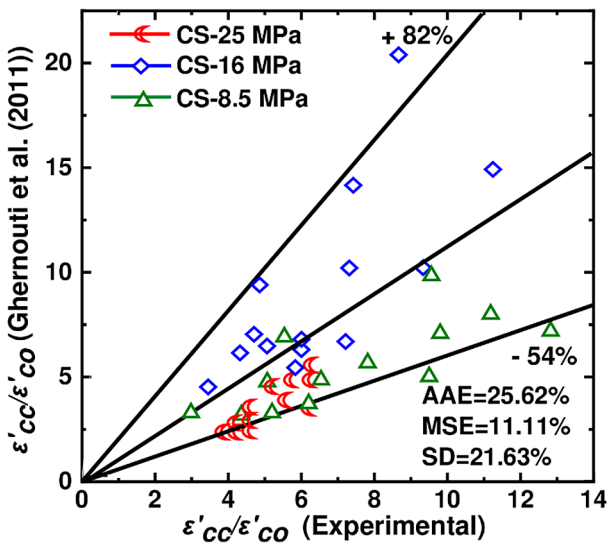

c) Ghernouti et al (2011)

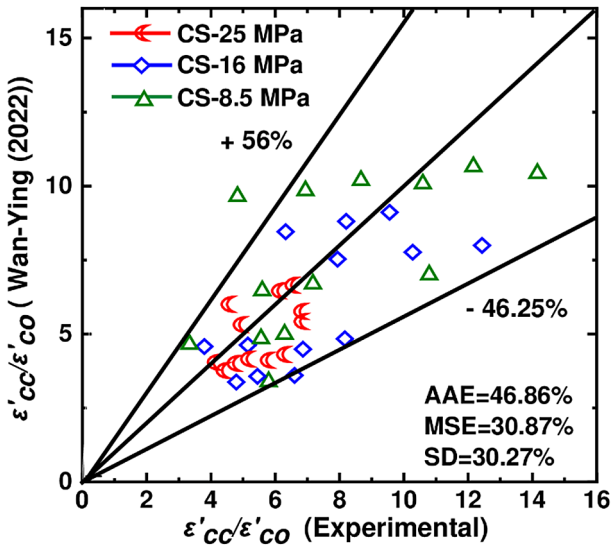

d) Wan-Ying 2022

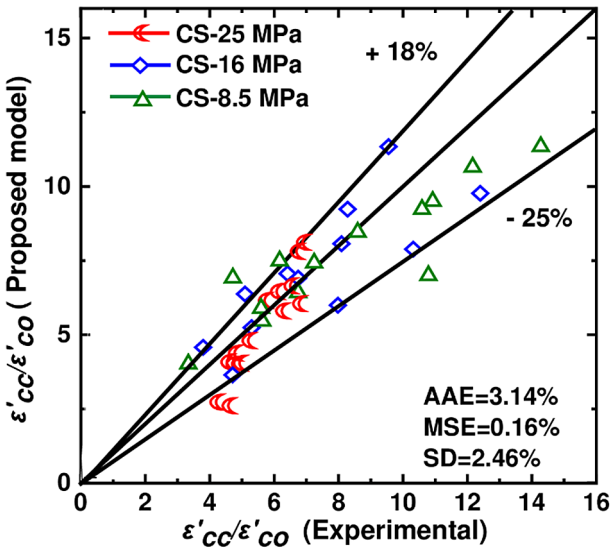

e) Proposed model

Figure 12. Comparison of the selected ultimate strain models with the experimental results.

these observations, the results are wildly inaccurate for predicting the ultimate strain. The predictions scatter for ultimate strain within a –25 to +18 margin for the proposed model.

As shown in Figure 12, most models can reasonably predict the behaviour of the GFCC confined in the GFRP. The models of Teng et al. (2007) [34], Benzaid et al. [33], Ghernouti and Rabehi [32], and Liao et al. [35] give (AAE = 32.6 %, MSE = 18.32 %, and SD = = 28.11 %), (AAE = 29.3 %, MSE = 14.7 %, and SD = = 25.08 %), (AAE = 25.6 %, MSE = 11.1 %, and SD = 21.6 %), (AAE = 46.8 %, MSE = 30.8 %, and SD = = 30.2 %), respectively. The statistical results overestimate the ultimate axial deformation. This is because all the ultimate axial strain models are based on the results of traditional strength concrete and the deformability of the GFRP confined GFCC is greatly affected by the

rupture strain of the internal and external FRP, but most of the models did not consider this factor. However, the proposed model gives AAE = 14.7 %, MSE= 3.47 %, and SD = 11.61 % and is able to provide accurate predictions.

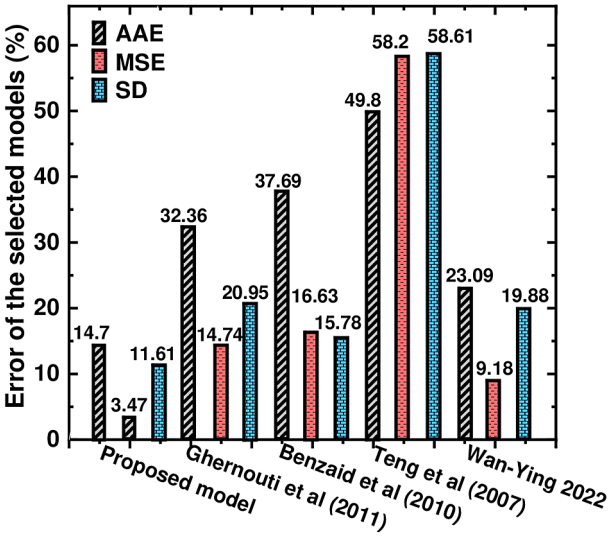

Figure 13. Evaluation of the parameters in predicting the normalised ultimate axial strain.

CONCLUSION

This research investigates the effects of the glass FRP content, concrete strength, and glass FRP thickness on the pure axial compression behaviour of extreme glass fibre reinforced concrete columns externally confined with locally available glass FRP composites. GFRC-GFRP confined concrete samples were tested for failure. Furthermore, the applicability of the proposed and existing models of the ultimate strength and strain is evaluated in this research.

On the one hand, the combined effect of the GFCC samples enveloped with a GFRP jacket reduces the lateral strain, and the confinement effect is independent of the glass fibre percentage and the concrete strength. By increasing the GFRP thickness, the confinement level significantly increases, leading to an increase in the ultimate strength of the GFCC-GFRP concrete. More importantly, a strain-softening behaviour characterises the GFCC specimens' responses, whereas the axial stress-strain responses of the GFRP confined samples exhibit an evident strain hardening behaviour.

On the other hand, the existing terminal stress models are poor for accurately predicting the ultimate stress of the GFCC-confined GFRP. Finally, the results show that the theoretical predictions of the models are close to the experimental results of high-strength GFCC, but not close to those of low-strength GFCC.

REFERENCES

1. Knoeri C., Sanyé-Mengual E., Althaus H.-J. (2013): Comparative LCA of recycled and conventional concrete for structural applications. *The International Journal of Life Cycle Assessment, 18*(5), 909–918. doi: 10.1007/s11367-012-0544-2
2. Farzad M., Shafieifar, M., Azizinamini A. (2019): Experimental and numerical study on bond strength between conventional concrete and Ultra High-Performance Concrete (UHPC). *Engineering Structures, 186*, 297–305. doi: 10.1016/j.engstruct.2019.02.030
3. Latifi M. R., Biricik, Ö., Mardani Aghabaglou A. (2021). Effect of the addition of polypropylene fiber on concrete properties. *Journal of Adhesion Science and Technology*, *36*(4), 345-369. doi: 10.1080/01694243.2021.1922221
4. Jiang C., Fan K., Wu F., Chen D. (2014): Experimental study on the mechanical properties and microstructure of chopped basalt fibre reinforced concrete. *Materials & Design, 58*, 187–193. doi: 10.1016/j.matdes.2014.01.056
5. Yao W., Li J., Wu K. (2003): Mechanical properties of hybrid fiber-reinforced concrete at low fiber volume fraction. *Cement and Concrete Research, 33*(1), 27–30. doi: 10.1016/s0008-8846(02)00913-4
6. Hefni Y., Zaher Y. A. E., Wahab M. A. (2018): Influence of activation of fly ash on the mechanical properties of concrete. *Construction and Building Materials, 172*, 728–734. doi: 10.1016/j.conbuildmat.2018.04.021
7. Aslani F., Hou L., Nejadi S., Sun J., Abbasi S. (2019): Experimental analysis of fiber-reinforced recycled aggregate self-compacting concrete using waste recycled concrete aggregates, polypropylene, and steel fibers. *Structural Concrete*, *20*(5), 1670-1683. doi:10.1002/suco.201800336
8. K Kytinou V., E Chalioris C., G Karayannis C., Elenas A. (2020): Effect of steel fibers on the hysteretic performance of concrete beams with steel reinforcement – Tests and analysis. *Materials, 13*(13), 2923. doi: 10.3390/ma13132923
9. Ren G., Gao X., Zhang H. (2022): Utilization of hybrid sisal and steel fibers to improve elevated temperature resistance of ultra-high performance concrete. *Cement and Concrete Composites, 130,* 104555. doi: 10.1016/j.cemconcomp.2022.104555.
10. Allam H., DuplanF., Amziane S., Burtschell Y. (2022): Assessment of manufacturing process efficiency in the dispersion of carbon fibers in smart concrete by measuring AC impedance. *Cement and Concrete Composites, 127*, 104394. doi: 10.1016/j.cemconcomp.2021.104394.
11. Karayannis C., Golias E., Kalogeropoulos G. I. (2022): Influence of Carbon Fiber-Reinforced Ropes Applied as External Diagonal Reinforcement on the Shear Deformation of RC Joints. *Fibers, 10*(3), 28. doi: 10.3390/fib10030028
12. Xu F., Wang S., Li T., Liu B., Li B., Zhou Y. (2020): Mechanical properties and pore structure of recycled aggregate concrete made with iron ore tailings and polypropylene fibers. *Journal of Building Engineering, 33*, 101572. doi: 10.1016/j.jobe.2020.101572
13. Canbaz M., Türeyen A. (2022): Effect of expanded polystyrene beads on the properties of foam concrete containing polypropylene fiber. *Challenge Journal of Concrete Research Letters, 13*(1), 28-35. doi: 10.20528/cjcrl.2022.01.003
14. Lian C., Wang Y., Liu S., Hao Y. (2021): Experimental Study of the Dynamic Compressive and Tensile Strengths

of Fly Ash and Slag Based Alkali-Activated Concrete Reinforced With Basalt Fibers. *Frontiers in Materals, 8*, 651581. doi: 10.3389/fmats.2021.651581

15. Sha H., Liu J. (2022): Static mechanical properties of reactive powder concrete reinforced with basalt fibers. *Structural Concrete, 23*, 1675-1686. doi: 10.1002/suco.202100746
16. Ali S., Sheikh M. N., NS Hadi M. (2021): Behavior of axially loaded plain and fiber-reinforced geopolymer concrete columns with glass fiber-reinforced polymer cages. Structural Concrete, 22(3), 1800-1816. doi: 10.1002/suco.202000231
17. Mohammed B. H., Sherwani A. F. H., Faraj R. H., Qadir H. H., Younis K. H. (2021): Mechanical properties and ductility behavior of ultra-high performance fiber reinforced concretes: Effect of low water-to-binder ratios and micro glass fibers. *Ain Shams Engineering Journal, 12*(2), 1557–1567. doi: 10.1016/j.asej.2020.11.008
18. Mendizabal V., Mercedes L., Bernat-Maso E., Gil L. (2022): Debonding of Vegetal FRCM from Concrete Beams Subjected to Bending Loads. *Key Engineering Materials, 916*, 449–456. doi: 10.4028/p-m59g07
19. Messas T., Achoura D., Abdelaziz B., Mamen B. (2022): Experimental investigation on the mechanical behavior of concrete reinforced with Alfa plant fibers. Frattura ed Integrità Strutturale, 16(60), 102-113. doi: 10.3221/IGF-ESIS.60.08
20. Ganesan N., Indira P. V., Sabeena M. V. (2014): Bond stress slip response of bars embedded in hybrid fibre reinforced high performance concrete. *Construction and Building Materials, 50*, 108–115. doi: 10.1016/j.conbuildmat.2013.09.032
21. Zheng D., Song W., Fu J., Xue G., Li J., Cao S. (2020): Research on mechanical characteristics, fractal dimension and internal structure of fiber reinforced concrete under uniaxial compression. *Construction and Building Materials, 258*, 120351. doi: 10.1016/j.conbuildmat.2020.120351
22. Guo Y., Hu X., Lv J. (2019): Experimental study on the resistance of basalt fibre-reinforced concrete to chloride penetration. *Construction and Building Materials, 223*, 142-155. doi: 10.1016/j.conbuildmat.2019.06.211
23. Niu D., Su L., Luo Y., Huang D., Luo D. (2020): Experimental study on mechanical properties and durability of basalt fiber reinforced coral aggregate concrete. *Construction and Building Materials, 237*, 117628. doi: 10.1016/j.conbuildmat.2019.117628
24. Lim J. C., Ozbakkaloglu T. (2015): Lateral strain-to-axial strain relationship of confined concrete. *Journal of Structural Engineering, 141*(5), 04014141. doi: 10.1061/(asce)st.1943-541x.0001094
25. Yin P., Huang L., Yan L., Zhu D. (2016): Compressive behavior of concrete confined by CFRP and transverse spiral reinforcement. Part A: experimental study. *Materials and Structures, 49*(3), 1001-1011. doi: 10.1617/s11527-015-0554-1
26. Ozbakkaloglu T., Gholampour A., Lim J. C. (2016): Damage-plasticity model for FRP-confined normal-strength and high-strength concrete. *Journal of Composites for Construction, 20*(6), 04016053. doi: 10.1061/(asce)cc.1943-5614.0000712
27. Pimanmas A., Saleem S. (2018): Dilation characteristics of PET FRP-confined concrete. *Journal of Composites for Construction, 22*(3), 04018006. doi: 10.1061/(asce)cc.1943-5614.0000841
28. Dai J. G., Bai Y. L., Teng J. G. (2011): Behavior and modeling of concrete confined with FRP composites of large deformability. *Journal of Composites for Construction, 15*(6), 963-973. doi: 10.1061/(asce)cc.1943-5614.0000230
29. ASTM (2010). D638-10 Standard test method for tensile properties of plastics. American Society for Testing and Materials, USA
30. Rodsin K., Hussain Q., Suparp S., Nawaz A. (2020): Compressive behavior of extremely low strength concrete confined with low-cost glass FRP composites. *Case Studies in Construction Materials, 13*, e00452. doi: 10.1016/j.cscm.2020.e00452
31. Raza A., ur Rehman A., Masood B., Hussain I. (2020): Finite element modelling and theoretical predictions of FRP-reinforced concrete columns confined with various FRP-tubes. *Structures, 26*, 626-638. doi: 10.1016/j.istruc.2020.04.033
32. Ghernouti Y., Rabehi B. (2011): FRP-confined short concrete columns under compressive loading: experimental and modeling investigation. *Journal of Reinforced Plastics and Composites, 30*(3), 241-255. doi: 10.1177/0731684410393054
33. Benzaid R., Mesbah H., Chikh N. E. (2010): FRP-confined concrete cylinders: axial compression experiments and strength model *Journal of Reinforced Plastics and Composites, 29*(16), 2469-2488. doi: 10.1177/0731684409355199
34. Teng J., Huang Y. L., Lam L., Ye L. P. (2007): Theoretical model for fiber-reinforced polymer-confined concrete. *Journal of Composites for Construction, 11*(2), 201-210. doi: 10.1061/(asce)1090-0268(2007)11:2(201)
35. Liao J., Zeng J. J., Jiang C., Li J. X., Yuan J. S. (2022): Stress-strain behavior and design-oriented model for FRP spiral strip-confined concrete. *Composite Structures, 293*, 115747. doi: 10.1016/j.compstruct.2022.115747